Meyer et al. Supplementary Figure S1

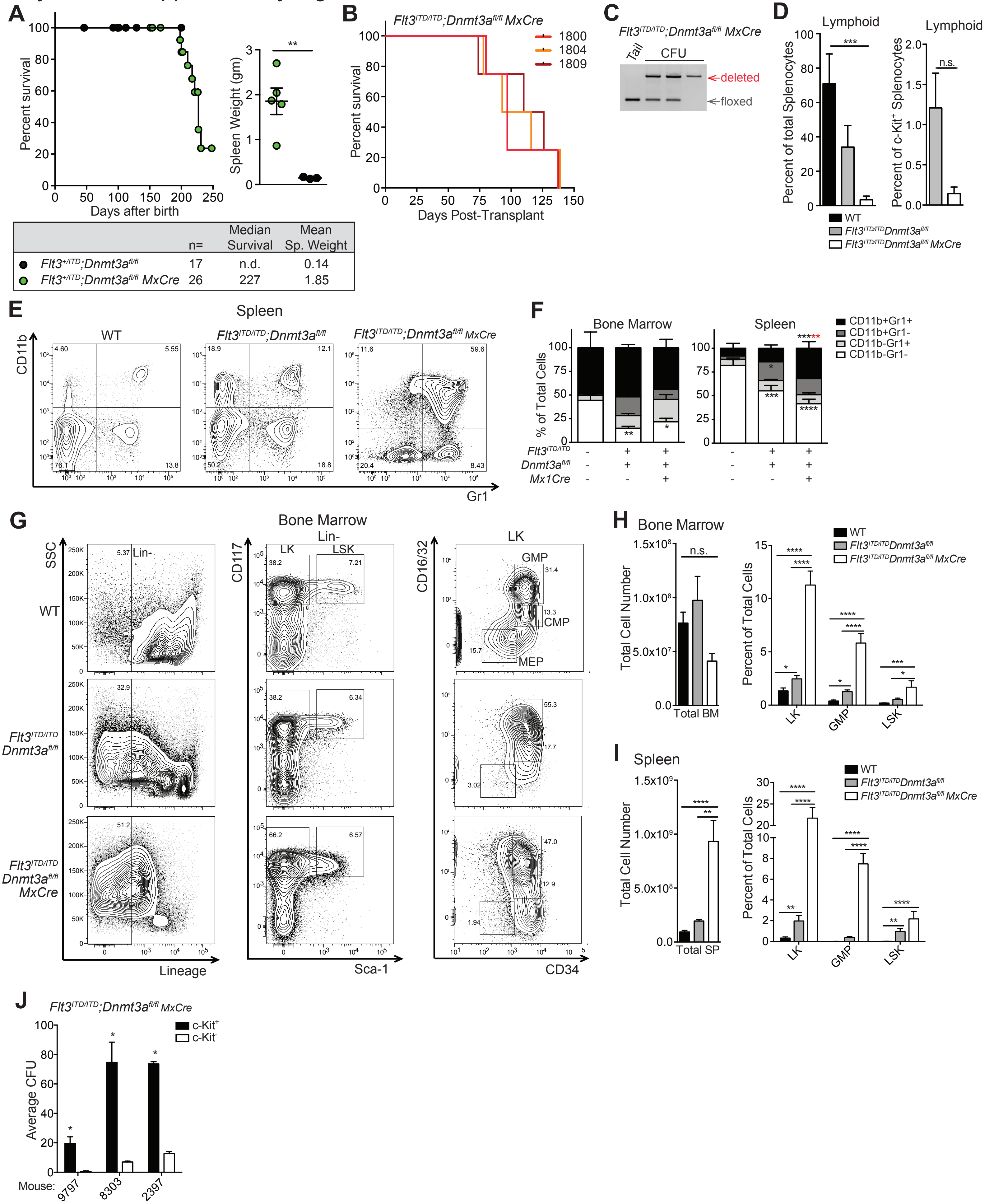

Supplementary Figure S1. *Dnmt3a* haploinsufficiency transforms *Flt3^{ITD}* MPN into an AML with clonogenic c-Kit^{+} leukemic stem and progenitors in the spleen. A, Kaplan-Meier survival curves (left) and spleen weights (right) of *Flt3$^{+/ITD}$Dnmt3a$^{fl/fl}$* mice without (black circles) and with *MxCre* (green circles). Table summarizes the number of animals, median survivals, and mean spleen weights of mice in study. Significant differences in survival were evaluated by Log-rank (Mantel-Cox) test and spleen weights by parametric unpaired t-test. **B,** Kaplan-Meier survival curves of recipient mice (n=4/donor) transplanted with equal numbers of total splenocytes purified from three independent primary *Flt3$^{ITD/ITD}$;Dnmt3a$^{fl/fl}$ MxCre* donor mice (numbered 1800, 1804, and 1809). **C,** Representative images of Dnmt3a floxed and deleted alleles by PCR on DNA from individual colonies derived from single c-Kit^{+} *Flt3$^{ITD/ITD}$;Dnmt3a$^{fl/fl}$ MxCre* splenocytes grown in methylcellulose for 7 days (right three lanes) and tail DNA as control (left lane). **D,** Frequencies ±SEM of total (left) and c-Kit^{+} (right) splenocytes expressing lymphoid markers CD3 or B220 derived from age-matched WT, *Flt3$^{ITD/ITD}$;Dnmt3a$^{fl/fl}$*, or *Flt3$^{ITD/ITD}$;Dnmt3a$^{fl/fl}$ MxCre* mice (at least 3 mice/group). Significant differences between the indicated populations were compared by one-way ANOVA multiple comparisons test (total splenocytes) or by unpaired parametric t-test (c-Kit^{+} splenocytes). **E-F,** Representative flow plots of spleen (**E**), and frequencies ±SEM (**F**) of bone marrow and spleen CD11b^{+}Gr1^{+} myeloid in age-matched wild-type (WT), *Flt3$^{ITD/ITD}$;Dnmt3a$^{fl/fl}$*, or *Flt3$^{ITD/ITD}$;Dnmt3a$^{fl/fl}$ MxCre* mice (at least 3 mice/group). Significant differences between the indicated populations were compared across all groups by two-way ANOVA Tukey's multiple comparisons test. Black asterisks indicate significant differences between *Flt3$^{ITD/ITD}$;Dnmt3a$^{fl/fl}$ MxCre* and WT; red asterisks indicate significant differences between *Flt3*$^{ITD/ITD}$*;Dnmt3a*$^{fl/fl}$ *MxCre* and *Flt3*$^{ITD/ITD}$*;Dnmt3a*$^{fl/fl}$. **G,** Representative flow plots of lineage negative (Lin$^-$), Lin$^-$c-Kit$^+$ (LK) and Lin$^-$Sca-1$^+$c-Kit$^+$ (LSK), and LK common myeloid progenitor (CMP)/ granulocyte-monocyte progenitor (GMP)/ megakaryocyte-erythroid progenitor (MEP) populations in bone marrow from WT, *Flt3*$^{ITD/ITD}$*;Dnmt3a*$^{fl/fl}$, or *Flt3*$^{ITD/ITD}$*;Dnmt3a*$^{fl/fl}$ *MxCre* mice. **H-I,** The total cellularity and frequencies ±SEM of LK, GMP, and LSK populations in bone marrow (**H**) and spleen (**I**) from age-matched WT, *Flt3*$^{ITD/ITD}$*;Dnmt3a*$^{fl/fl}$, or *Flt3*$^{ITD/ITD}$*;Dnmt3a*$^{fl/fl}$ *MxCre* mice (at least 5 mice/group). Significant differences between populations were compared across all groups by two-way ANOVA Tukey's multiple comparisons test. **J,** Average ±SEM number of colonies arising from c-Kit$^+$ (black bars) or c-Kit$^-$ (white bars) splenocytes from three independent *Flt3*$^{ITD/ITD}$*;Dnmt3a*$^{fl/fl}$ *MxCre* mice after 7 days in methylcellulose. Significant differences were determined by Holm-Šídák multiple comparisons t-tests. In all panels where indicated *p≤0.05, **p≤0.01, ***p≤0.001, and ****p≤0.0001.

Meyer et al. Supplementary Figure S2

Supplementary Figure S2. Comparative patterns of differential global DNA methylation in *DNMT3A*-mutant human and murine AML. A-F, Ideograms depicting regions of differentially hypermethylated (pink) and hypomethylated (green) DNA along each chromosome in human (**A-C**) and murine (**D-F**) samples. Comparisons indicated at the top of each ideogram. Comparing normal human HSC to human *FLT*3-ITD *DNMT3A*-WT AML (**A**) or human *FLT*3-ITD *DNMT3A*-mutant AML (**B**) reveals changes associated with malignancy; however, direct comparison of human *FLT*3-ITD *DNMT3A*-WT AML versus *FLT*3-ITD *DNMT3A*-mutant AML (**C**) reveals concise global changes associated with *DNMT3A* mutation. Similarly, comparison of normal murine LSK with murine *FLT3*-ITD MPN (**D**) or *FLT3*-ITD *Dnmt3a*-mutant AML (**E**) reveals changes associated with FLT3-ITD transformation; however, direct comparison of murine *FLT3*-ITD MPN and *FLT3*-ITD *Dnmt3a*-mutant AML (**F**) reveals concise global changes associated with *Dnmt3a* mutation.

Meyer et al. Supplementary Figure S3

A

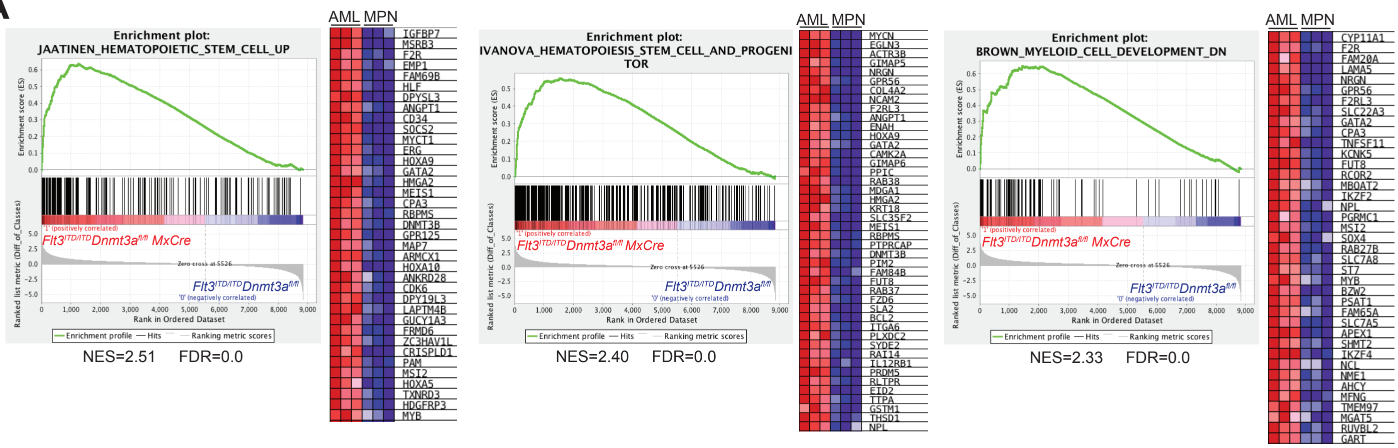

B

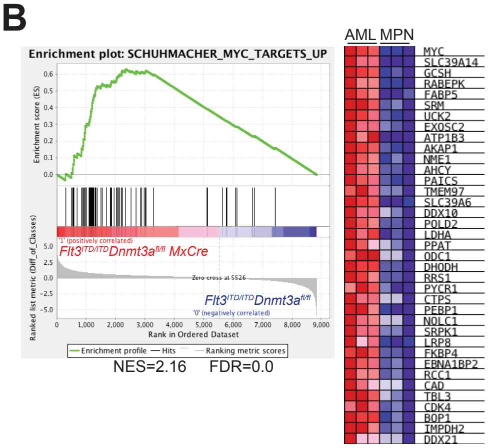

Supplementary Figure S3. Hematopoietic stem cells/progenitor and c-Myc signatures are upregulated in murine AML. GSEA analyses query of the MSigDB were performed using descending ranked fold change expression of *Flt3*$^{ITD/ITD}$*;Dnmt3a*$^{fl/fl}$ *MxCre* AML compared to *Flt3*$^{ITD/ITD}$*;Dnmt3a*$^{fl/fl}$ MPN. **A,** Hematopoietic stem cell/progenitor upregulated gene sets (left and middle) and myeloid cell development downregulated gene sets (right) were amongst the top-enriched gene sets associated with genes upregulated in the murine *Flt3*$^{ITD/ITD}$*;Dnmt3a*$^{fl/fl}$ *MxCre* AML compared to MPN models. **B,** Enrichment for gene sets associated c-Myc regulated targets were upregulated in murine *Flt3*$^{ITD/ITD}$*;Dnmt3a*$^{fl/fl}$ *MxCre* AML compared to MPN RNA-Seq.

Meyer et al. Supplementary Figure S4

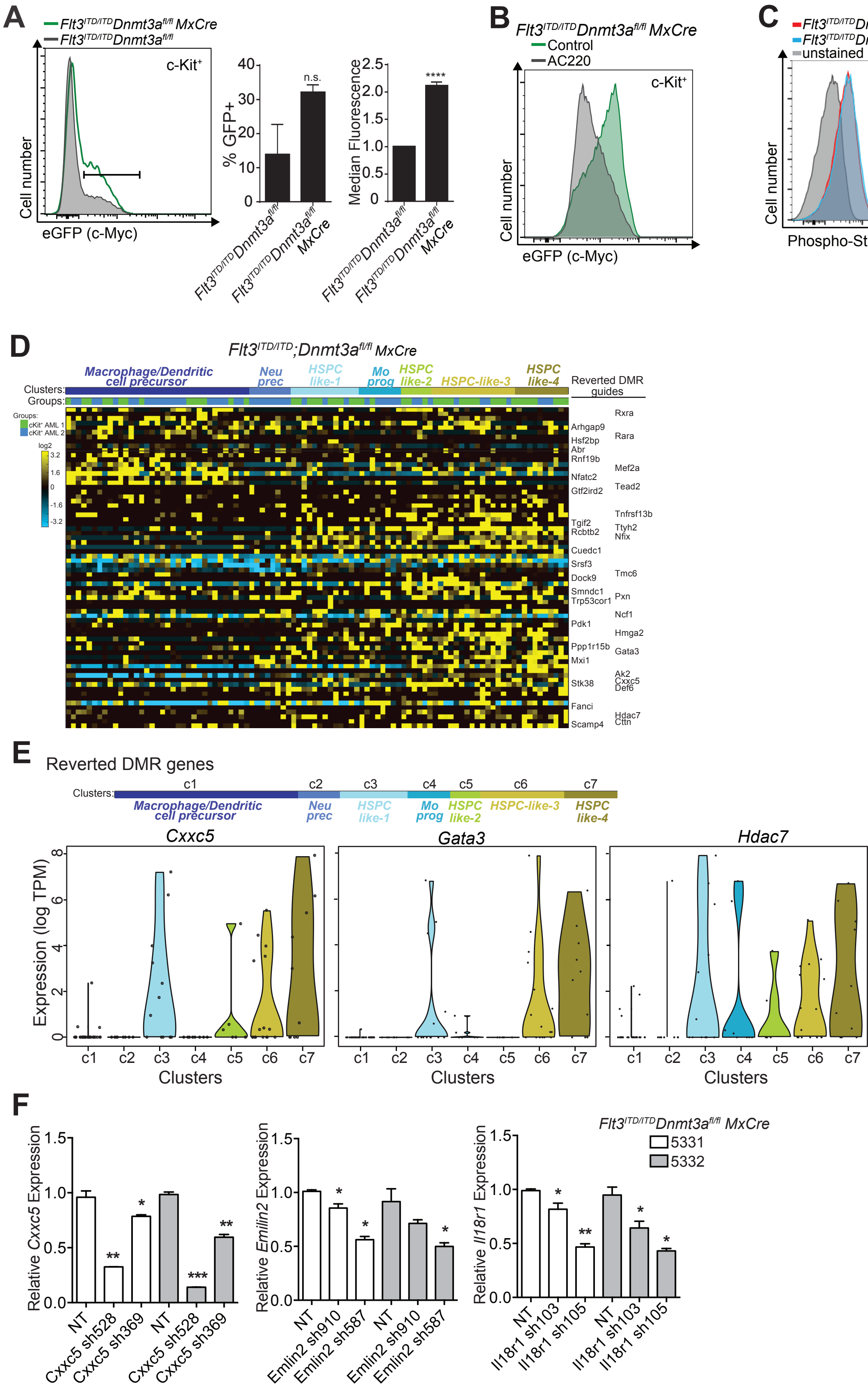

Supplementary Figure S4. DNMT3A rescued murine *Flt3*$^{ITD/ITD}$*;Dnmt3a*$^{fl/fl}$ *MxCre* AML hypermethylated regions correspond to HSPC-like populations. A, Representative histograms of c-Myc (eGFP) expression in the c-Kit^{+} splenocyte fraction from *c-Myc*^{eGFP}*;Flt3*$^{ITD/ITD}$*;Dnmt3a*$^{fl/fl}$ *MxCre* AML (green line) and *c-Myc*^{eGFP}*;Flt3*$^{ITD/ITD}$*;Dnmt3a*$^{fl/fl}$ MPN (gray line) mice. Average frequency ±SEM (left bar graph) of c-Kit^{+}eGFP^{+} and median eGFP fluorescence intensity (right bar graph) in c-Kit^{+} cells from *c-Myc*^{eGFP}*;Flt3*$^{ITD/ITD}$*;Dnmt3a*$^{fl/fl}$ MPN and *c-Myc*^{eGFP}*;Flt3*$^{ITD/ITD}$*;Dnmt3a*$^{fl/fl}$ *MxCre* AML are reported for at least 3 mice/group. Statistical significance was evaluated by unpaired parametric t-test (****$p \leq 0.0001$). **B,** Representative histogram of c-Myc (eGFP) expression in murine *c-Myc*^{eGFP}*;Flt3*$^{ITD/ITD}$*;Dnmt3a*$^{fl/fl}$ *MxCre* AML cells treated with AC220 or vehicle control. **C,** Representative histogram (left) and median fluorescence intensity (MFI) (right bar graph) of phosphorylated Stat5 (phospho-Stat5) intracellular flow analyses in c-Kit^{+} cells from *Flt3*$^{ITD/ITD}$*;Dnmt3a*$^{fl/fl}$ MPN and *Flt3*$^{ITD/ITD}$*;Dnmt3a*$^{fl/fl}$ *MxCre* AML are reported for at least 3 mice/group. No statistical differences were found between AML and MPN for phospho-Stat5 by unpaired parametric t-test. **D,** Heatmap of scRNA-Seq data showing expression of genes associated with genomic regions that were hypomethylated in *Flt3*$^{ITD/ITD}$*;Dnmt3a*$^{fl/fl}$ *MxCre* AML (compared to MPN) and hypermethylated upon DNMT3A rescue. Rank cell order maintained from **Fig. 3A**, and ICGS clusters are shown at the top. **E,** Violin plots of *Cxxc5*, *Gata3*, and *Hdac7* from panel **D** for the mean gene expression differences in each of the ICGS clusters. **F,** Average ±SEM expression of *Cxxc5*, *Emilin2*, and *Il18r1* in corresponding shRNA or non-targeting (NT) control transduced *Flt3*$^{ITD/ITD}$*;Dnmt3a*$^{fl/fl}$ *MxCre* AML cells derived from two independent tumors (mouse AML # 5331; white bars, mouse AML # 5332;gray bars). Expression is shown as relative to NT control for each mouse. *Sdha* served as loading control. Significance was evaluated by unpaired parametric t-test compared to the NT control for each mouse, respectively (*$p \leq 0.05$, **$p \leq 0.01$, ***$p \leq 0.001$).

Supplementary Table Legends

Supplementary Table S1. Peripheral blood findings in moribund *Flt3*$^{ITD/ITD}$*;Dnmt3a*$^{fl/fl}$ *MxCre* mice and age-matched *Flt3*$^{ITD/ITD}$*;Dnmt3a*$^{fl/fl}$ and wild-type control mice.

Supplementary Table S2. Frequencies of monocyte and myelomonocytic populations in the bone marrow and spleen of *Flt3*$^{ITD/ITD}$*;Dnmt3a*$^{fl/fl}$ *MxCre* mice and age-matched *Flt3*$^{ITD/ITD}$*;Dnmt3a*$^{fl/fl}$ and wild-type control mice by flow cytometric analyses.

Supplementary Table S3. Differentially methylated regions (DMR) in human *FLT3*-ITD/*DNMT3A*-mut versus *FLT3*-ITD/*DNMT3A*-wt AML and in murine *Flt3*$^{ITD/ITD}$*;Dnmt3a*$^{fl/fl}$ *MxCre* AML versus *Flt3*$^{ITD/ITD}$*;Dnmt3a*$^{fl/fl}$ MPN control mice. Lists of AML-unique and HSPC-like DMR associated genes in human and mouse based on DMRs found only in the *Dnmt3a* mutant AML groups or DMRs in *Dnmt3a* mutant AML with similar methylation patterns to normal HSC.

Supplementary Table S4. RNA-Seq gene expression analyses of *Flt3*$^{ITD/ITD}$*;Dnmt3a*$^{fl/fl}$ *MxCre* AML versus *Flt3*$^{ITD/ITD}$*;Dnmt3a*$^{fl/fl}$ MPN and comparison of differentially expressed genes to human *FLT3*-ITD/*DNMT3A*-mut gene expression and murine AML DMR by GSEA. Lists of AML-unique and HSPC-like genes in human and mouse based on deregulated gene expression found only in the *Dnmt3a* mutant AML groups or deregulated gene expression in *Dnmt3a* mutant AML with similar deregulation patterns to normal HSC.

Supplementary Table S5. ICGS HOPACH gene expression clustering results performed on RNA-Seq data from 96 single *Flt3*$^{ITD/ITD}$*;Dnmt3a*$^{fl/fl}$ *MxCre* AML cells.

Supplementary Table S6. DMR in DNMT3A rescued c-Kit+ *Flt3*$^{ITD/ITD}$*;Dnmt3a*$^{fl/fl}$ *MxCre* cells versus c-Kit+ *Flt3*$^{ITD/ITD}$*;Dnmt3a*$^{fl/fl}$ *MxCre* empty vector control cells.

Supplementary Table S7. Clinical mutation data on primary human AML samples.